

Quench dynamics of Rydberg dressed bosons on two-dimensional square lattices

Yijia Zhou,¹ Yongqiang Li,^{2,3} Rejish Nath,⁴ and Weibin Li^{1,5}

¹*School of Physics and Astronomy, University of Nottingham, Nottingham NG7 2RD, United Kingdom*

²*Department of Physics, National University of Defense Technology, Changsha 410073, P. R. China*

³*Department of Physics, Graduate School of China Academy of Engineering Physics, Beijing 100193, P. R. China*

⁴*Indian Institute of Science Education and Research, Pune 411 008, India*

⁵*Centre for the Mathematics and Theoretical Physics of Quantum Non-Equilibrium Systems, University of Nottingham, Nottingham NG7 2RD, United Kingdom*

(Dated: September 2, 2022)

We study dynamics of bosonic atoms on a two dimensional square lattice, where atomic interactions are long ranged with either a box or soft-core shape. The latter can be realized through laser dressing ground state atoms to electronically excited Rydberg states. When the range of interactions is equal or larger than the lattice constant, the system is governed by an extended Bose-Hubbard model. We propose a quench process by varying the atomic hopping linearly across phase boundaries of the Mott insulator-supersolid and supersolid-superfluid phases. Starting from a Mott insulator state, dynamical evolution exhibits a universal behaviour at the early stage. We numerically find that the universality is largely independent of interactions during this stage. However, dynamical evolution could be significantly altered by long-range interactions at later times. We demonstrate that density wave excitations are important below a critical quench rate, where non-universal dynamics is found. We also show that the quench dynamics can be analysed through time-of-flight images, i.e. measuring the momentum distribution and noise correlations.

I. INTRODUCTION

In the past decades, there has been a growing interest in the study of ultracold atoms, which is largely driven by the unprecedented level of control over external trapping potentials, internal states and interactions between atoms with electromagnetic fields [1–9]. Various lattice models [10], such as the Bose-Hubbard model [11], have been studied and realized experimentally [12]. This has opened opportunities to probe static properties [13–15], such as Mott insulator-superfluid phase transition [11, 12, 16, 17], spin-orbit coupling [18–20], supersolidity [21–30], entanglement [31, 32], topology [33, 34], etc. The advantage of cold atom systems is that many parameters can be manipulated and monitored dynamically. This has paved new ways to explore non-equilibrium dynamics in addition to static properties. Inspired by this, recent theoretical and experimental works have investigated Landau-Zener transition [35–37], Kibble-Zurek mechanism [38–44], transport [45–47], Higgs/Goldstone modes [48, 49].

Recently, growing interest has been spent on investigating dynamics of Bose-Hubbard models (BHMs) driven by external periodic [50, 51] or linear fields [52]. A recent review can be found in Refs. [53, 54]. A particularly interesting topic is the universal evolution of the BHM when linearly changing the hopping strength. Many quantities, such as dynamical correlation length and topological defects, can be scaled with respect to the change (quench) rate of the hopping, which are rooted from the Kibble-Zurek mechanism (KZM) [38–41]. The universality originates from the fact that the system evolution is frozen around the phase boundary while adiabatic away from it.

In uniform Bose-Hubbard models (BHMs), the competition between the hopping and two-body on-site inter-

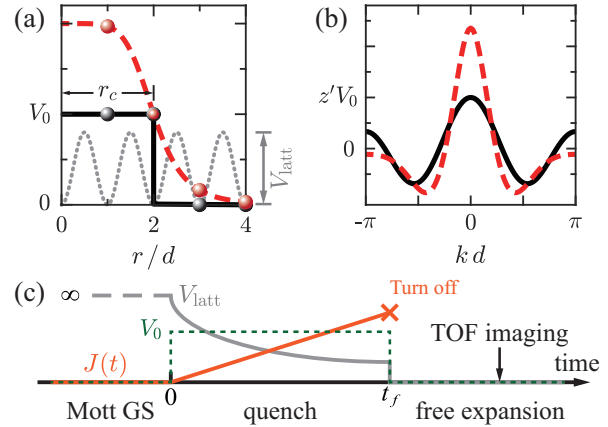


FIG. 1. **Long-range interaction and quench scheme.** (a) Long-range soft-core (red dashed) and box-type (black solid) interaction. The range r_c of interactions can be longer than the optical lattice (dotted) constant d . (b) Fourier transform of the interaction potential. The line style is same as shown in panel (a). (c) Quench protocol. At $t < 0$, we prepare the ground state in a Mott insulator with $V_{\text{latt}} \rightarrow \infty$ and $J = 0$. The tunnelling $J(t)/U = a_Q t$ (orange) is increased linearly during $t \in (0, t_f)$. This is done by reducing lattice depth (grey). At the same time, long-range interactions (green dotted) is turned on. When $t > t_f$, atoms are released from the optical lattice.

actions [55–57] leads to a Mott insulator (MI) to superfluid (SF) phase transition at a critical hopping. In extended Bose-Hubbard models (eBHMs), where the range of atomic interactions is longer than the lattice constant, ground state can have non-uniform, periodic densities, such as the density wave (DW), supersolid (SS), Haldane insulator (HI in 1D), etc [58, 59]. Such situation

has been examined extensively using atoms with weak magnetic or electric dipole moments [60–68], where the dominant interaction is between nearest neighbour sites. When quenching eBHM, the nearest-neighbour interaction will bring extra time scales [42, 43]. It was found that vortex nucleation and correlation lengths exhibit different scaling laws other than that in BHM.

In this work, we will go beyond the nearest-neighbour interaction regime and examine eBHM with even longer range interactions. This is realized by using Rydberg dressed atoms confined in a two dimensional optical lattice [6–9, 69–73]. Rydberg atoms have long lifetimes ($\sim n^3$), where $n \gg 1$ is the principal quantum number. Large polarizabilities ($\sim n^7$) give strong and long-range interactions (e.g. van der Waals interactions $\sim n^{11}$) between Rydberg atoms. However atomic hopping typically occurs on a much slower time scale than the Rydberg lifetime. One could instead weakly couple ground state atoms to Rydberg states with a large detuned laser [69, 74–76]. This results to a soft-core shape potential between Rydberg dressed ground state atoms. Its range could extend several lattice constants before decaying significantly (see Fig. 1a). The range of the soft-core interaction is characterized by a radius r_c . For distance $r < r_c$, the interaction strength is nearly a constant, while decays quickly if $r > r_c$. Such a interaction potential may be approximated by a box potential, i.e. atomic interaction is a constant when $r \leq r_c$ and zero otherwise (Fig. 1a). Box-type interactions have been used to study the extended Bose-Hubbard model, with a focus on nearest-neighbour cases ($r_c = d$) [27, 58, 59]. They share similar profiles in momentum space (Fig. 1b). We will show that the underlying dynamics show common features for these two types of interactions.

This paper is organized as follows. In Sec. II we introduce the eBHM of the Rydberg dressed atoms. We show the relation between the roton instability and density modulations. In Sec. III, we discuss universal dynamics of the phase transition on the boundary of MI phase, by examining global variables including SF fraction ρ_s and density variance σ_n . In Sec. IV, we propose that the dynamics can be measured through TOF density distribution [28, 68, 77] and covariance [57, 78–82]. These quantities will change with the probe time. In Sec. V, differences between soft-core interaction and the simplified box-type interaction are discussed. We conclude in Sec. VI.

II. EXTENDED BOSE-HUBBARD MODEL

The Hamiltonian of the Rydberg dressed atoms in the 2D square lattice is given by an eBHM [21–23, 27, 28, 58],

$$H = -J(t) \sum_{\langle ij \rangle} \hat{b}_i^\dagger \hat{b}_j + \frac{U}{2} \sum_i \hat{n}_i (\hat{n}_i - 1) + \sum_{i \neq j} V_{ij} \hat{n}_i \hat{n}_j, \quad (1)$$

where $\langle ij \rangle$ stands for the nearest-neighbour sites, and $J(t)$ is the time-dependent hopping. U is the on-site

interaction, including contributions from s-wave scattering and the long-range interaction. In this work, two types of long-range interactions are considered. The soft-core interaction between Rydberg atoms is $V_{ij} = 2V_0[1 + (r_{ij}/r_c)^6]^{-1}$, where r_{ij} is the distance between site i and j , r_c is the soft-core radius, and V_0 is the interaction strength. In case of a box potential, the interaction is given by $V_{ij} = V_0 \Theta(r_c - r_{ij})$, where $\Theta(r)$ is the Heaviside function (Fig. 1a). The situation that we will particularly focus on is that the initial state has an unit filling, i.e. $\langle n_i \rangle = \langle b_i^\dagger b_i \rangle = 1$.

The SS and SF phase boundary is approximately determined by examining instabilities of the Bogoliubov spectra [83, 84],

$$E(\mathbf{k}) = \sqrt{\varepsilon(\mathbf{k})^2 + \rho_0 \varepsilon(\mathbf{k}) (U + \tilde{V}(\mathbf{k}))}, \quad (2)$$

where $\varepsilon(\mathbf{k}) = 2J(2 - \cos(k_x d) - \cos(k_y d))$ is the kinetic energy term, ρ_0 is the condensate density and $\tilde{V}(\mathbf{k}) = \frac{1}{M} \sum_{i \neq j} V_{ij} \exp(i\mathbf{k} \cdot \mathbf{r}_{ij})$, is the Fourier component of long-range interaction. In free space, $\tilde{V}(\mathbf{k})$ has analytical solutions, which yields $\tilde{V}(\mathbf{k}) = V_0 \frac{2\pi r_c}{|\mathbf{k}|} J_1(|\mathbf{k}|r_c)$ for box-type interaction and $\tilde{V}(\mathbf{k}) = V_0 \frac{4\pi r_c^2}{3} \sum_{m=0, \pm 1} e^{i2m\pi/3} K_0(e^{im\pi/3} |\mathbf{k}| r_c)$ for soft-core interactions, where $J_n(x)$ is the first kind of Bessel function and $K_n(x)$ is the second kind of modified Bessel function [85]. In the two-dimensional lattice, we numerically calculate the Fourier transform of the interaction potential (see Fig. 1b).

For strong long-range interactions, the many-body ground state could have non-uniform, periodic densities [74, 86, 87]. The onset of non-uniform densities is signified by unstable Bogoliubov spectra. This allows us to determine a critical hopping for so-called roton instability $J_l = -\min[\Sigma(\mathbf{k})]$, where

$$\Sigma(\mathbf{k}) = \rho_0 \frac{U + \tilde{V}(\mathbf{k})}{2 - \cos(k_x d) - \cos(k_y d)}. \quad (3)$$

Such that when $J_s < J < J_l$, the density modulation will occur, where J_s is the phase boundary of MI. A typical shape of $\Sigma(\mathbf{k})$ is shown in Fig. 2a. The roton instabilities are presented in Bogoliubov spectra as the white areas in Fig. 2b. Through numerical fitting of J_l versus V_0 , we find that its slope for the soft-core interaction becomes larger than the box potential when increasing the interaction range r_c . On the other hand, momentum \mathbf{k}_{rot} corresponding to the onset of roton instabilities varies with the soft-core radius r_c . From the numerical data, one finds that $|\mathbf{k}_{\text{rot}}| \approx 3\pi/2r_c$ when $r_c \gg d$ (Fig. 2d).

To implement the quench, the hopping strength changes according to $J(t)/U = a_Q t$ for $t \in [0, t_f]$ (see Fig. 1c). Typically the system is in the SF region at the final $J(t_f)$. Without long-range interactions (i.e. in BHM), the phase boundary in the unit-filled 2D square lattice is $J_s/U = 0.0429$ with decoupling approach [16] and 0.059 with quantum Monte-Carlo calculation [88]. In

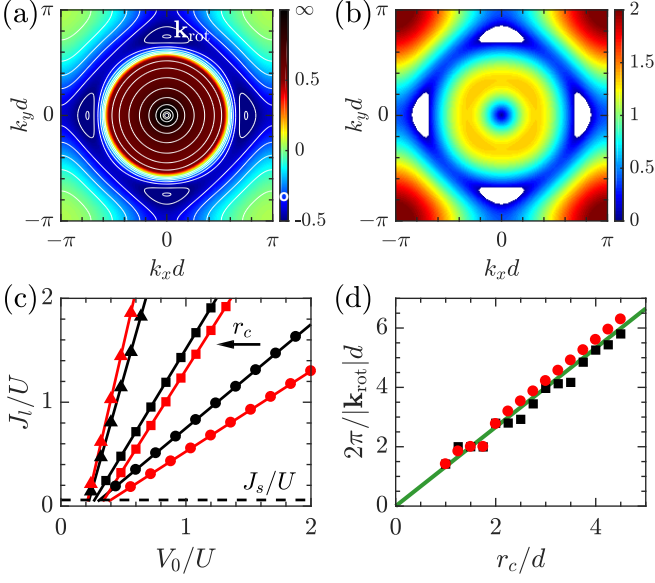


FIG. 2. **Roton instability.** (a) $\Sigma(\mathbf{k})$ as defined in Eq. (3). The momentum \mathbf{k}_{rot} is found at the minimal $\Sigma(\mathbf{k})$ when the spectra become complex. (b) Bogoliubov spectra for $J = 0.5U$. The white areas indicate roton instability. In (a) and (b) we consider the soft-core interaction with $r_c = 2d$ and $V_0 = 0.6U$. (c) Critical tunnelling J_l for box-type (black) and soft-core (red) interactions. The arrow shows that the slope increases as r_c grows. The soft-core length is $r_c/d = 1$ (dot), 2 (square), and 3 (triangle). (d) Momentum $|\mathbf{k}_{\text{rot}}|$ at the roton minimum, in term of its inverse, for box-type (square) and soft-core (dot) interactions. Here the interaction strength is $V_0 = 2U$.

this case, $J(t_f)$ will be larger than both values to ensure that the system enters the SF region.

We employ the time-dependent Gutzwiller method [89–92] to simulate the dynamics. Expanding the many-body wave function as $|\Psi_N\rangle \approx \Pi_i |\Psi_i\rangle$, where the wave function of i -th site is expanded to Fock basis as $\Psi_i = \sum_m f_m^i(t) |i; m\rangle$. The equation of motion of coefficients f_m^i is given by

$$i \frac{\partial}{\partial t} f_m^i = -J(t) \sum_{r_{ij}=1} \left(\sqrt{m} \phi_j f_{m-1}^i + \sqrt{m+1} \phi_j^* f_{m+1}^i \right) + \left(\frac{U}{2} m(m-1) + m \sum_{j \neq i} V_{ij} n_j \right) f_m^i, \quad (4)$$

where $\phi_i = \langle \hat{b}_i \rangle$ is the SF order parameter. The initial state is a MI ground state with homogeneous occupation $n_i = 1$, and random phase is applied to coefficients f_m^i to take into account of initial coherence [39].

III. QUENCH DYNAMICAL WITH BOX-TYPE INTERACTIONS

In this section, we study response to the linear increasing $J(t)$ with the box-type interaction. We will

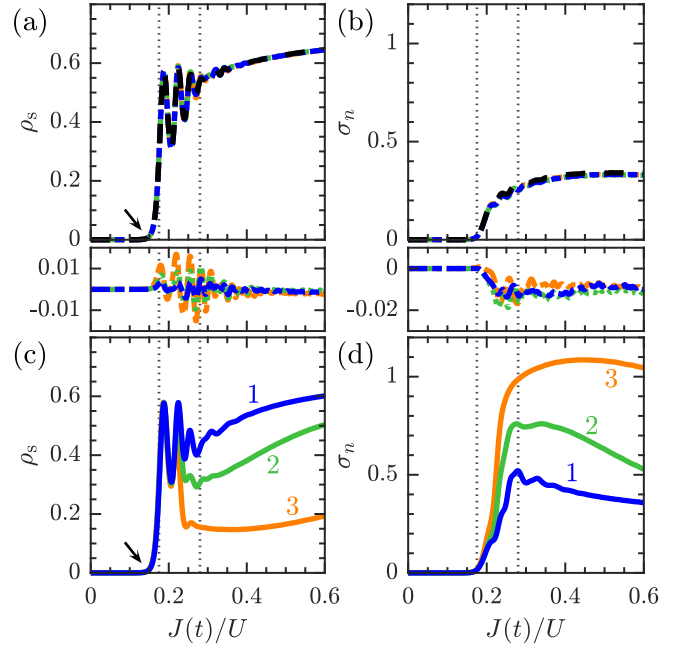


FIG. 3. **Superfluid fraction ρ_s (a,c) and density variance σ_n (b,d) with box-type interactions.** In weak interacting cases (a,b), we consider $V_0 = 0$ (dashed black) and $V_0/U = 0.1$ (coloured). The lower panel shows the difference of ρ_s and σ_n between interacting and non-interacting cases. In strong interacting cases (c,d), the evolution apparently depends on the strength and radius of the long-range interaction. For all of the plots, we consider $V_0/U = 0.5$, $a_Q/U = 0.01$ and $r_c/d = \{1$ (blue), 2 (green), 3 (orange) $\}$. The quench rate. Dotted lines indicate probe times for time-of-flight (TOF) interference. Arrows indicate the Kibble-Zurek time. See text for details.

investigate quantities such as superfluid fraction $\rho_s = \sum_{\langle i,j \rangle} \text{Re}[\phi_i^* \phi_j]/zM$ [93, 94], density variance $\sigma_n = \sum_i \sqrt{\langle \hat{n}_i^2 \rangle - \langle \hat{n}_i \rangle^2}/M$ and vortex nucleations. Here $z = 4$ is the coordination number of 2D square lattice, M is the total number of lattice points. In the MI phase ($J(t)/U \ll 1$), both ρ_s and σ_n vanish.

A. Superfluid fraction, density variance and vortex density

When the long-range interaction is weak, the dynamics is largely similar to that of the BHM, as shown in Fig. 3a,b. Initially both ρ_s and σ_n remain small with increasing $J(t)$ with rate $a_Q/U = 0.01$. During this stage, atom tunnelling is negligible until $J(t)$ increases to $\sim 0.17U$. Then ρ_s and σ_n increase rapidly. The importance of the value $\hat{J}/U \approx 0.17$ is related to the Kibble-Zurek mechanism, which will be investigated in the next section. Here the long-range interaction acts as a weak perturbation on top of the strong on-site interaction (see lower panel of Fig. 3a,b, where the difference between interacting and non-interacting cases are plotted).

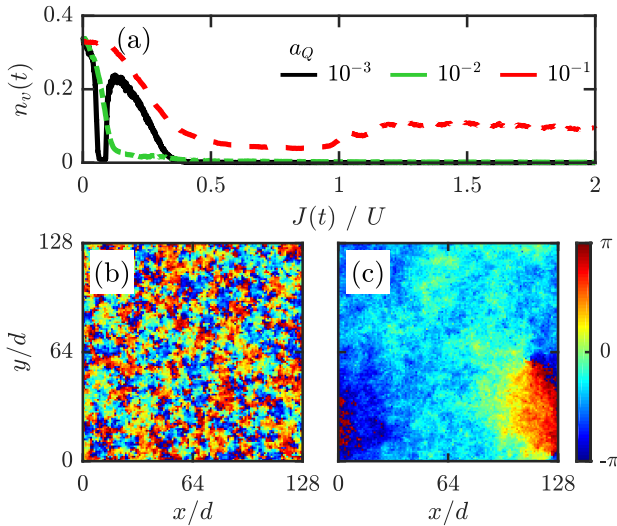


FIG. 4. Vortex nucleation with box-type interaction. (a) Evolution of vortex density with box-type interactions with $V_0/U = 0.5$, $r_c = d$, $J(t_f)/U = 2$. The quench rate a_Q/U is 10^{-3} (black), 10^{-2} (green), 10^{-1} (red). The local phase of SF order parameter $\arg(\phi)$ at $J(t_f) = 2$ is shown for (b) $a_Q/U = 10^{-1}$, $U t_f = 20$ and (c) $a_Q/U = 10^{-3}$, $U t_f = 2000$.

Dynamics changes drastically at different stages when the long-range interactions becomes stronger, as illustrated in Fig. 3c and d. At early times, values of ρ_s are independent of the long-range interaction. However ρ_s changes significantly at later times. Its values decrease with increasing soft-core length r_c . The evolution of σ_n is more sensitive to r_c . We find different curves depart from each other even at a relatively early stage. Interestingly, larger superfluid fraction usually results in larger density fluctuation, but we find that σ_n becomes larger for larger r_c at later times, though ρ_s is reduced. The margin between weak and strong interaction is caused by the roton excitation in the latter.

We now turn to the discussion of the vortex nucleation. When $J(t)$ is increased, topological defects (vortices) can be created due to phase transition. The development of the topological defects in the vicinity of phase transition point is related to quantities such as the healing length, density fluctuation, etc as found in BHM [39] and eBHM with dipolar interactions [25, 68]. In our system, the vortex density all starts around $n_v \approx 1/3$ (Fig. 4a), which is a result of the initial state where local phases are purely random. The vortex density decreases slowly for the fast quench. This suggests the system has no time to relax and the initial excitation is carried forward by the time-dependent state. The fast increasing hopping inhibits the unification of local phases. As shown in Fig. 4b, many vortices still survive in this deep SF regime.

Decreasing the quench rate to $a_Q/U = 0.01$, the initial vortex density decays dramatically with time, and n_v

begins to vanish around $J(t)/U = 0.17$. Interestingly, a new regime emerges when the quench rate is further decreased. At $a_Q/U = 10^{-3}$, we find that the vortex density first decreases rapidly, then increases quickly after $J(t) = 0.071U$ and then slowly decreases with increasing $J(t)$. The revival of the vortex density here is attributed to the strong and long-range interaction. As the dynamics is nearly adiabatic, initial noises decays rapidly. With increasing hopping, the interplay between atomic tunnelling and interaction creates a lot of vortex nucleations in the system. When $J(t)$ is large, the system is relaxed to a homogeneous SF with only a few vortex nucleations (Fig. 4c).

B. Kibble-Zurek dynamics

The key feature of KZM in a BHM is that dynamics is divided into frozen and adiabatic region across the phase transition. It is convenient to define a *distance parameter* $\epsilon = J(t)/J_s - 1$, which depends on the critical hopping J_s of the MI-SF transition. Dynamics is qualitatively different before and after a frozen parameter $\hat{\epsilon}$. As the instantaneous relaxation time $\tau(t)$ diverges around the phase transition, dynamics of system is frozen to the initial state if $|\epsilon| < \hat{\epsilon}$. However, dynamical evolution becomes adiabatic when $|\epsilon| > \hat{\epsilon}$, where many dynamical quantities change significantly. The relaxation time can be estimated by KZM for $\tau = |\epsilon/\hat{\epsilon}|$. On the other hand, Landau's mean field theory predicts that $\tau = \tau_0|\epsilon|^{-z\nu}$, where ν is the critical exponent about correlation length, τ_0 is a coefficient of relaxation time for BHM, and z is the dynamical exponent. This permits us to find the frozen parameter and frozen (KZM) time [39],

$$\hat{\epsilon} = \left(\frac{a_Q \tau_0}{J_s/U} \right)^{\frac{1}{1+z\nu}}, \quad \hat{t} = \frac{J_s/U}{a_Q} \left(\frac{a_Q \tau_0}{J_s/U} \right)^{\frac{1}{1+z\nu}}. \quad (5)$$

In practice, it is difficult to determine the KZM time from numerical calculations. In this work, we estimate the time when $d^2\rho_s/dt^2$ is maximized (indicated by arrows in Fig. 3a,c). Other choices, e.g., in Shimizu, *et al*'s work the KZM time is chosen to be the time when $|\phi(t_0 + \hat{t})| = 2|\phi(t_0)|$ [41], will make minor difference in τ_0 , but the scaling exponents remain the same.

To find the universal laws in ρ_s , we change the quench rate from 10^{-3} to 10^{-1} , and find the KZM time for non-interacting, box-type and soft-core interactions with $V_0/U = 0.6$, $r_c = d, 2d$, respectively. The corresponding distance parameter $\hat{\epsilon}$ is shown in Fig. 5a. Apparently $\hat{t}(\hat{\epsilon})$ is independent to the interaction types. The data can be described by a single set of fitting parameters $J_s/U = 0.0449$, $z\nu = 0.442$ and $U\tau_0 = 21.0$. Our fitted J_s is closer to the decoupling approach ($J_s/U = 0.043$) [16].

KZM also predicts that the vortex density $n_v \sim \xi^{\text{def}}/\xi^{\text{dim}} \sim a_Q^{(\text{dim}-\text{def})\nu/(1+z\nu)}$, where ξ is the correlation length, and $\text{dim} = 2$ is the dimension of the lattice, def is

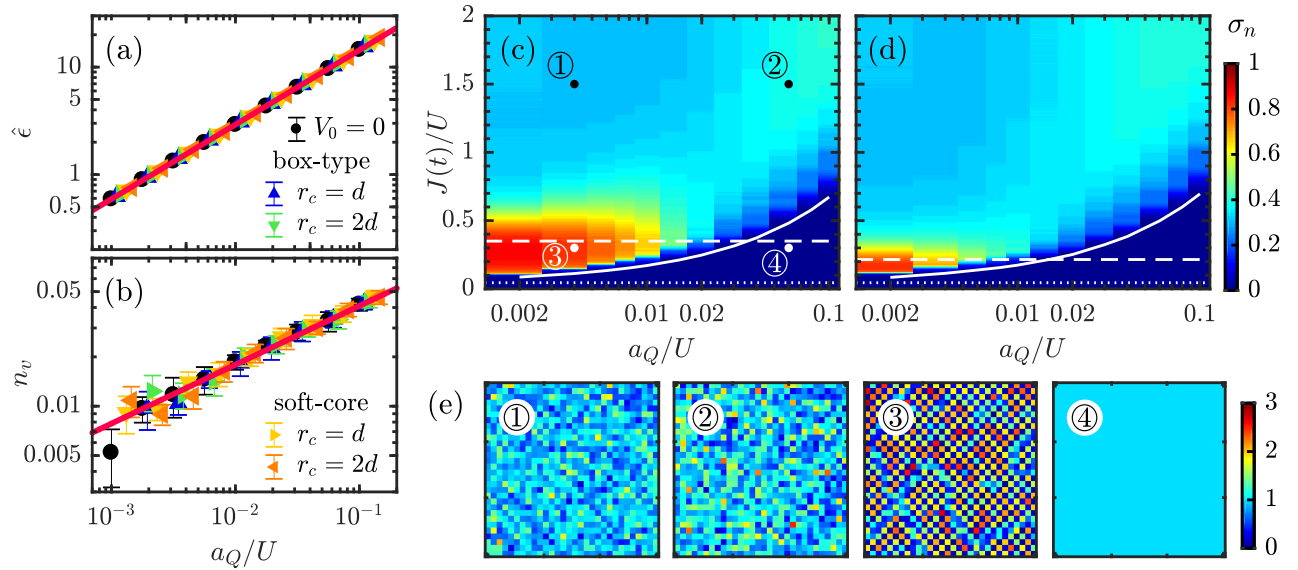


FIG. 5. **Kibble-Zurek mechanism and a comparison with roton instability.** Dynamics of global variables by using box-type and soft-core interaction. (a) Kibble-Zurek time, in term of distance parameter $\hat{\epsilon}$, fitted from the turning point of superfluid fraction. The interaction configurations include non-interacting (black), box-type with $V_0/U = 0.6$ and $r_c = d$ (blue), $r_c = 2d$ (green), soft-core with $V_0/U = 0.6$ and $r_c = d$ (yellow), $r_c = 2d$ (orange). (b) Density of vortices counted at Kibble-Zurek time from the fitting results. Density variance σ_n with respect to hopping $J(t)$ with box-type (c) and soft-core (d) interaction for both $r_c = d$ and $V_0/U = 0.6$. The hopping parameter at KZM time $J(\hat{t})$ (solid line), roton instability J_l (dashed line) and MI-SF transition of BHM J_s (dotted line) are plotted together. (e) Density distributions of specific quench rate and time with box-type interaction shown in (c), where ① $a_Q/U = 0.004$, $J(t)/U = 1.5$, ② $a_Q/U = 0.06$, $J(t)/U = 1.5$, ③ $a_Q/U = 0.004$, $J(t)/U = 0.3$, ④ $a_Q/U = 0.06$, $J(t)/U = 0.3$.

that of topological defects. Here we argue that $\text{def} = 1$ because the vortices are always created in pairs (e.g., Fig. 4c). Numerically, in 2D square lattice, n_v can be evaluated according to $n_v = 1/(4M) \sum_i |\sin(\theta_{i+\hat{x}} - \theta_i) + \sin(\theta_{i+\hat{x}+\hat{y}} - \theta_{i+\hat{x}}) + \sin(\theta_{i+\hat{y}} - \theta_{i+\hat{x}+\hat{y}}) + \sin(\theta_i - \theta_{i+\hat{y}})|$, where $\theta_i = \arg(\phi_i)$. Using the same interaction configuration as aforementioned, we found that the scaling exponent $(\text{dim} - \text{def})\nu/(1+z\nu) = 0.359$ as shown in Fig. 5b. Compared to the fitting results of $\hat{\epsilon}$, we found $\nu = 0.518$, $z = 0.854$. Here we make a comparison with mean-field class where $\nu = 0.5$, $z = 2$, and 3D XY model, which is frequently compared with 2D BHM, where $\nu = 2/3$ and $z = 1$ [11, 95, 96]. In Ref. [41], it was found that the vortex density has anomalous behaviour in slow quench regime ($a_Q/U < 10^{-2}$). In our simulations, n_v shows larger fluctuation as a_Q decreases, but the average values still fit well with the universal scaling. This is mainly a result of finite size effect.

It is apparent that the onset of roton instabilities breaks the universal dynamics at later times. This is more apparent for slow quenches, where the tunnelling $J(\hat{t})$ at the Kibble-Zurek time \hat{t} is smaller than the tunnelling J_l for the roton instability. For fast quenches when $J(\hat{t}) > J_l$, however, the system will not fully respond to the roton mode, where dynamics is still universal. To demonstrate this, we calculate the density variance σ_n , shown in Fig. 5c-e. The density variance develops a maximal value around $J(t) \sim J_l$ when the

quench rate is low. In this region, the system suffers significantly from the roton instability, exhibiting apparent density patterns (Fig. 5e3). When $J(\hat{t}) > J_l$, the density variance σ_n increases slowly with time. This shows that we can estimate the transition from non-universal to universal dynamics by a quench rate a_c at which $J(\hat{t}) \approx J_l$.

IV. TIME-OF-FLIGHT ANALYSIS

Through analyzing the momentum distribution and noise correlations [78, 80–82], we can identify phases of the system dynamically by releasing the optical lattice [28, 57, 68, 77, 79, 81, 97] at different quench times. Interference patterns are determined by the quasi-momentum distribution after TOF, which encodes information of SF order parameters. In deep SF regime, the momentum distribution $n(\mathbf{k}) = \langle \hat{b}_{\mathbf{k}}^\dagger \hat{b}_{\mathbf{k}} \rangle$, $\hat{b}_{\mathbf{k}}$ being the bosonic operator in momentum space, is approximately

$$n(\mathbf{k}) \approx |\tilde{\phi}_{\mathbf{k}}|^2, \quad (6)$$

where $\tilde{\phi}_{\mathbf{k}} = 1/\sqrt{M} \sum_i \phi_i \exp[i\mathbf{k} \cdot \mathbf{r}_i]$ is the Fourier component of the SF order parameter ϕ_i , M is the number of lattice points.

Non-uniform density structures [84] can be characterized by the noise correlation, which is obtained through HBT-type interference measurements. We calculate the covariance $C(\mathbf{k}, \mathbf{k}') = \langle \hat{b}_{\mathbf{k}}^\dagger \hat{b}_{\mathbf{k}} \hat{b}_{\mathbf{k}'}^\dagger \hat{b}_{\mathbf{k}'} \rangle - \langle \hat{b}_{\mathbf{k}}^\dagger \hat{b}_{\mathbf{k}} \rangle \langle \hat{b}_{\mathbf{k}'}^\dagger \hat{b}_{\mathbf{k}'} \rangle$, which

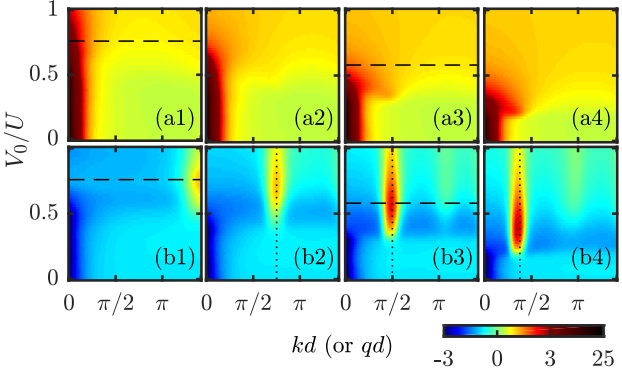


FIG. 6. **Effects of interaction length and strength revealed in TOF experiments.** Momentum density $n(k)$ (a1-a4) and covariance $C(q)$ (b1-b4). The probe time is $Ut = 28$ with quench rate $a_Q/U = 0.01$. We consider box-type interaction with strengths $V_0 \in [0, U]$, and radius $r_c/d = \{1, 2, 3, 4\}$ from left to right, respectively. Dotted lines indicate the momentum where the covariance has maximal values. Two dimensional plots corresponding to interactions given by dashed black lines are shown in Fig. 8.

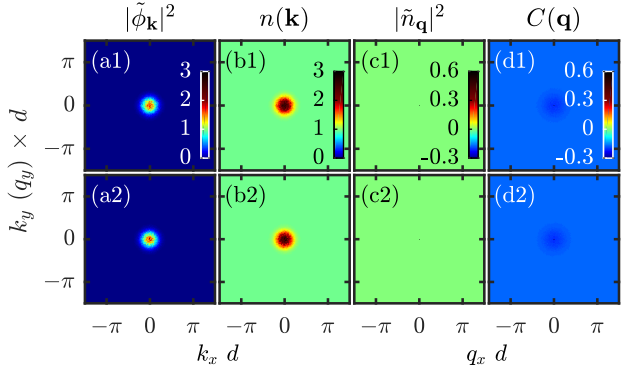


FIG. 7. **Snapshots at early time $Ut = 17.5$ with quench rate $a_Q/U = 0.01$.** TOF density $n(\mathbf{k})$ (b1-b2) and covariance $C(\mathbf{q})$ (d1-d2) are compared with the Fourier transform of order parameter $\tilde{\phi}_{\mathbf{k}}$ (a1-a2) and density $\tilde{n}_{\mathbf{q}}$ (c1-c2). (a1-d1) is that without long-range interaction, and (a2-d2) for box-type interaction with $r_c = d$ and $V_0/U = 0.66$.

can be reduced to a function of relative momentum $\mathbf{q} = \mathbf{k}' - \mathbf{k}$ in deep MI regime, that approximately yields

$$C(\mathbf{q}) \approx |\tilde{n}_{\mathbf{q}}|^2, \quad (7)$$

where $\tilde{n}_{\mathbf{q}}$ is the Fourier component of occupation n_i similar to $\tilde{\phi}_{\mathbf{k}}$. The analytical expressions for $n(\mathbf{k})$ and $C(\mathbf{k}, \mathbf{k}')$ are presented in the Appendix, modified from Ref. [57, 78, 81].

We will illustrate that instantaneous features at different times will be vastly different. In previous sections, we have shown that system dynamics is largely frozen up to the Kibble-Zurek time. In Fig. 7, we find that $\tilde{\phi}_{\mathbf{k}}$ and $n(\mathbf{k})$ are almost uniform except a small peak area around the $\mathbf{k} = 0$. Such feature is hardly visible in the distri-

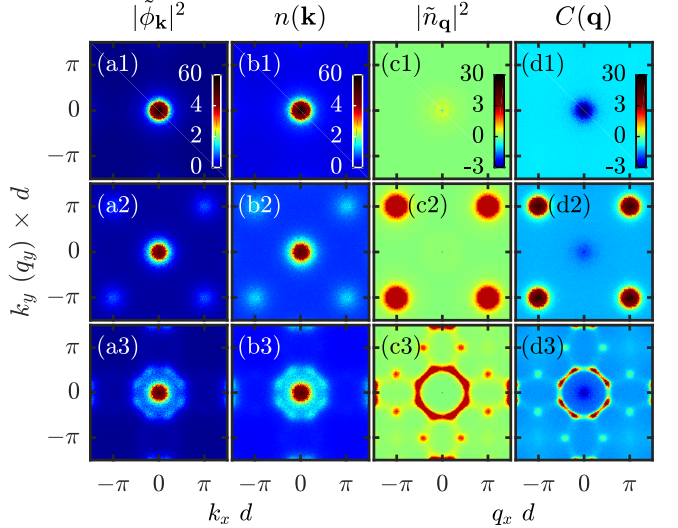


FIG. 8. **Snapshots at late time $Ut = 28$ with quench rate $a_Q/U = 0.01$.** TOF density $n(\mathbf{k})$ (b1-b3) and covariance $C(\mathbf{q})$ (d1-d3) are compared with the Fourier transform of order parameter $\tilde{\phi}_{\mathbf{k}}$ (a1-a3) and density $\tilde{n}_{\mathbf{q}}$ (c1-c3). Interactions are box-type and their lengths from the top to bottom $r_c/d = \{0$ (non-interacting), 1, 3 $\}$, strengths $V_0/U = \{0, 0.66, 0.36\}$.

bution of $\tilde{n}_{\mathbf{q}}$ and $C(\mathbf{q})$. Note that all these distributions are flat in the initial state.

At a later time (see Fig. 3), dynamics is strongly different from the initial stage. The radial distribution of the momentum $n(k)$ and covariance $C(q)$ are shown in Fig. 6a1-a4, and b1-b4, respectively. For weak long-range interactions, $n(k)$ has a strong peak around $k = 0$, signifying the appearance of the SF phase. When the soft-core width is small, widths of the momentum distribution decreases slowly with increasing interaction strength (Fig. 6a1). Here rotons are excited at large momentum (Fig. 6b2), around $\sqrt{2}\pi/r_c$ (factor $\sqrt{2}$ is due to the 2D square lattice, see Fig. 8 for details). However the roton excitation is weak and only perturbs the momentum distribution. When the radius is large, the momentum distribution is strongly affected by non-negligible roton excitation (see Fig. 6b3) with stronger long-range interactions. The appearance of the roton minima at nonzero momentum causes a flat dispersion relation, which gives a very broad momentum distribution (Fig. 6a3).

To reveal details of the data shown in Fig. 6, we calculate $\tilde{\phi}_{\mathbf{k}}$ and $\tilde{n}_{\mathbf{q}}$, i.e. Fourier transformation of the order parameter and spatial density. Distributions of these two quantities together with $n(\mathbf{k})$ and $C(\mathbf{q})$ are shown in Fig. 8. In the SF regime, the distributions are more visible in $\tilde{\phi}_{\mathbf{k}}$ and $n(\mathbf{k})$ where a peak is found around $|\mathbf{k}| = 0$ (the 1st row in Fig. 8). For stronger interactions, peaks at different momentum are found (the 2nd and 3rd rows in Fig. 8). These peaks are more profound in the Fourier transformation of the density and covariance where the central peaks are suppressed. For example, four peaks

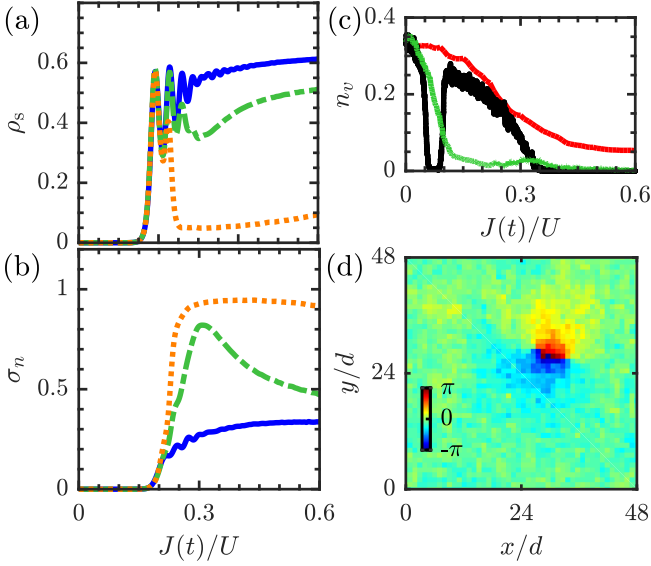


FIG. 9. **Dynamics of superfluid fraction ρ_s (a), density variance σ_n (b) and vortex nucleation (c-d) for soft-core interactions.** (a-b), the soft-core radius is $r_c/d = 2.5$ and quench rate $a_Q/U = 0.01$. The interaction strengths are $V_0/U = 0.1$ (blue), 0.5 (green), 0.8 (yellow). (c) Density of vortices under different quench rate $a_Q/U = 10^{-1}$ (red), 10^{-2} (green), 10^{-3} (black). The interaction strength is $V_0/U = 0.5$, radius $r_c/d = 2.5$. (d) The phase of local SF order parameter $\arg(\phi)$ at $J(t_f) = 2U$ with $a_Q/U = 10^{-3}$.

are found at $|k_x|d = |k_y|d = \pi$ in the second row. These positions are determined by the soft-core radius. For nearest-neighbor [28] we find the peak is around $\pi d/r_c$. Increasing the soft-core radius, more and more peaks are found (see the 3rd row), as the long-range interactions overlap with lattice sites of different distances. Hence one can obtain the positions by looking at properties of elliptical lattices within the soft-core radius.

V. SOFT-CORE INTERACTION

The more realistic soft-core interaction have a similar shape as the box potential at short distances. The long-range tail decays quickly with distances. We first show that the qualitative phenomena are the same as discussed before. Here we demonstrate this with parameters $r_c/d = 2.5$, $V_0/U = 0.1, 0.5, 0.8$, $a_Q/U = 0.01$, and the global variables ρ_s and σ_n are evaluated as shown in Fig. 9a,b. When V_0 is small, the dynamics is again similar to non-interacting case. But as V_0 grows larger, ρ_s will decrease and σ_n increases. The margin between weak and strong interaction estimated by roton instability is $\approx 0.29U$. When $V_0/U = 0.8$, the drop of ρ_s and rise of σ_n becomes stronger, and the relaxation time also grows.

The evolution of vortices with varying quench rate is

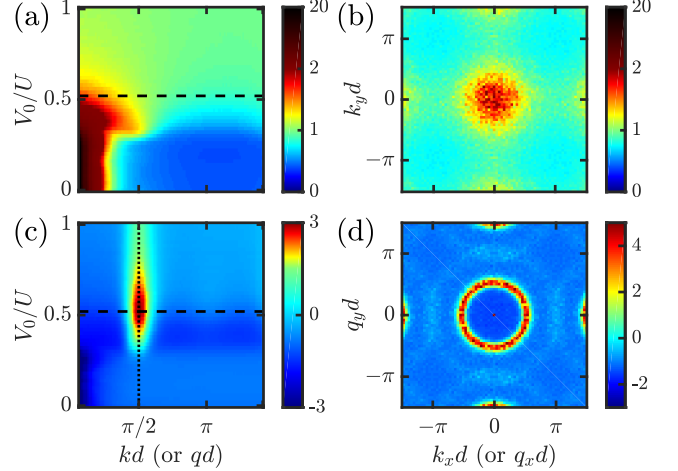


FIG. 10. **TOF imaging and covariance analysis for soft-core interaction.** The soft-core radius $r_c = 3d$, quench rate $a_Q/U = 0.01$, and probe time $Ut = 28$. TOF density $n(\mathbf{k})$ for (a) ring integral and (b) at $V_0/U = 0.36$. Covariance $C(\mathbf{q})$ for (c) ring integral and (d) at $V_0/U = 0.36$. The dotted vertical line is the predicted momentum of roton minimum.

shown in Fig. 9c. Compared to Fig. 4, the basic profile is the same. The notable difference is that the decay of n_v becomes relatively faster as a_Q decreases. But when a_Q is too small, there is also a sudden revival of vortex nucleation. The final phase of SF order of $a_Q/U = 10^{-3}$ is plotted in Fig. 9d.

The qualitative similarity between box-type and soft-core interaction lies on their interaction strength and length. As shown in Fig. 2a, the soft-core interaction has the same magnitude at $r = r_c$ and is non-zero at $r > r_c$. Fig. 2c shows that the boundary cause roton instability is similar for box-type and soft-core interactions, which suggests that the dominant point is $V(r = r_c)$. This accounts for our definition where a factor of 2 is introduced.

However the tail of the soft-core interaction affects the time-of-flight results. As shown in Fig. 10a,c, the strength that facilitate density structures is similar to Fig. 6b2,b3, and the positions of the peaks of $C(\mathbf{q})$ also agree with roton instability analysis. However, the patterns of covariance is significantly different. For box-type interaction with $r_c = 3d$, $C(\mathbf{q})$ has an octupole geometry. In soft-core case, however, more wave numbers are taken into account such that the peaks has much less contrast over the ring $|\mathbf{q}| = |\mathbf{k}_{\text{rot}}|$. The large interference peak in $n(\mathbf{k})$ promises that there is non-zero tunnelling in the length scale of density patterns. The second order density structure in Fig. 8d3 becomes much faded in Fig. 10d. This suggests that local density distribution is not much supported by soft-core interactions.

VI. CONCLUSION

In this paper we studied dynamical properties of an two-dimensional eBHM by quenching the atomic hopping. The dependency to long-range interactions and quench rates are examined in detail. We find that the stability of a uniform SF will be destroyed by the presence of strong and long-range interactions. This leads to a new SS phase between the MI and SF region. When quenching the hopping from an initial MI phase, the dynamics is universal at the early stage. This frozen dynamics is explained using the Kibble-Zurek mechanism. After that, the order parameter rises quickly with time (hopping). For weaker interactions, we observe universal dynamics even after the onset of the SF order parameters. This is changed drastically when the long-range interaction is strong, giving rise to non-negligible SS order parameters. The system eventually enters the SF regime when the hopping is large enough, where a small number of vortices can still survive. We also proposed TOF experiments to measure the quench dynamics and determine effects induced by long-range interactions.

In the future, it is worth to exploring situations that are relevant to current cold atom experiments. One could investigate roles played by dimensionality (1D, 3D) and lattice structures (triangular, honeycomb, etc) in the dynamics of the Rydberg dressed gases. Another interesting question is on the quench dynamics induced by time-dependent long-range interactions. This can be realized experimentally by (adiabatically or abruptly) turning on the Rydberg dressing laser [72]. Starting from a SF, this permits us to understand, e.g. dynamics of quantum depletion in the presence of long-range interactions.

ACKNOWLEDGMENTS

We thank Huaizhi Wu and Mark Fromhold for many useful comments. This work is supported from the UKIERI-UGC Thematic Partnership No. IND/CONT/G/16-17/73, EPSRC Grant No. EP/M014266/1 and EP/R04340X/1, Indo-French Centre for the Promotion of Advanced Research, National Natural Science Foundation of China under Grants No. 11304386 and 11774428. The numerical simulation

is carried out at the University of Nottingham High Performance Computing Facility. We also thank the support of the University of Nottingham through a RPA grant and China Scholarship Council.

Appendix A: Time-of-flight interference and noise correlation

In the time-of-flight experiments, the atomic motion is nearly governed by ballistic expansion. Therefore, the field operator at space-time $\{t; \mathbf{x}\}$ yields $\hat{b}_{\mathbf{k}} = \tilde{w}(\mathbf{k}) \sum_i \hat{b}_i \exp[i\mathbf{k} \cdot \mathbf{r}_i]$ with $\mathbf{k} = m\mathbf{x}/(\hbar t)$. Here $\tilde{w}(\mathbf{k})$ is the Fourier component of Wannier function of the lowest band of the optical lattice. We make an assumption that the optical lattice is deep enough such that $|\tilde{w}(\mathbf{k})| \approx \text{const.}$ Under Gutzwiller approximation, the expectation value of density operator $n(\mathbf{k}) = \langle \hat{n}_{\mathbf{k}} \rangle = \langle \hat{b}_{\mathbf{k}}^\dagger \hat{b}_{\mathbf{k}} \rangle$ reads

$$n(\mathbf{k}) = |\tilde{w}(\mathbf{k})|^2 + \frac{1}{M} \sum_i (n_i - |\phi_i|^2). \quad (\text{A1})$$

Compared to Eq. 6, the second term in Eq. (A1) is a constant, which preserves the total number of atoms.

Similarly, the full expression for the covariance $C(\mathbf{k}, \mathbf{k}') = \langle \hat{n}_{\mathbf{k}} \hat{n}_{\mathbf{k}'} \rangle - \langle \hat{n}_{\mathbf{k}} \rangle \langle \hat{n}_{\mathbf{k}'} \rangle$ reads

$$\begin{aligned} C(\mathbf{k}, \mathbf{k}') = & |F(n - |\phi|^2; \mathbf{q})|^2 + |F(\eta^* - \phi^{*2}; \mathbf{Q})|^2 + \\ & \Delta(\mathbf{q})F(n - |\phi|^2; \mathbf{q}) - 4X(\phi^*; (n - |\phi|^2)\phi) + \\ & 2X(\phi^*; \gamma - \eta\phi^*) + \sqrt{M}\Delta(\mathbf{q})F(\phi^*; \mathbf{k})\tilde{F}(\phi; \mathbf{k}') + \\ & + 2\sqrt{M} \left[Y(\phi, \phi, \eta^* - \phi^{*2}; \mathbf{k}, \mathbf{k}') + \right. \\ & \left. Y(n - |\phi|^2, \phi, \phi^*; \mathbf{q}, \mathbf{k}) \right] + \frac{C_0}{M}, \end{aligned} \quad (\text{A2})$$

where $\mathbf{q} = \mathbf{k}' - \mathbf{k}$, $\mathbf{Q} = \mathbf{k}' + \mathbf{k}$, and $\eta_i = \langle \hat{b}_i \hat{b}_i \rangle$, $\gamma_i = \langle \hat{b}_i^\dagger \hat{b}_i \hat{b}_i \rangle$, $\lambda_i = \langle \hat{b}_i^\dagger \hat{b}_i^\dagger \hat{b}_i \hat{b}_i \rangle$. $F(\tilde{F})$ represents for the (inverse) Fourier transformation, and $\Delta(\mathbf{q}) = 1/\sqrt{M} \sum_i \exp[i\mathbf{q} \cdot \mathbf{r}_i]$, $X(f, g) = \text{Re}[F(f; \mathbf{k})\tilde{F}(g; \mathbf{k}) + F(f; \mathbf{k}')\tilde{F}(g; \mathbf{k}')]$, $Y(f, g, h; \mathbf{k}_1, \mathbf{k}_2) = \text{Re}[F(f; \mathbf{k}_1)F(g; \mathbf{k}_2)\tilde{F}(h; \mathbf{k}_1 + \mathbf{k}_2)]$, $C_0 = \sum_i (8n_i|\phi_i|^2 - 2n_i^2 - |\eta_i|^2 + \lambda_i - 6|\phi_i|^4 - 4\text{Re}[\gamma_i^* \phi_i - \eta_i^* \phi_i^2])$.

[1] D. Jaksch, C. Bruder, J. I. Cirac, C. W. Gardiner, and P. Zoller, *Phys. Rev. Lett.* **81**, 3108 (1998).

[2] J. Stenger, S. Inouye, M. R. Andrews, H. J. Miesner, D. M. Stamper-Kurn, and W. Ketterle, *Phys. Rev. Lett.* **82**, 2422 (1999).

[3] M. Theis, G. Thalhammer, K. Winkler, M. Hellwig, G. Ruff, R. Grimm, and J. H. Denschlag, *Phys. Rev. Lett.* **93**, 123001 (2004).

[4] C. Chin, R. Grimm, P. Julienne, and E. Tiesinga, *Rev. Mod. Phys.* **82**, 1225 (2010).

[5] J. Schachenmayer, I. Lesanovsky, A. Micheli, and A. J. Daley, *New J. Phys.* **12**, 103044 (2010).

[6] J. E. Johnson and S. L. Rolston, *Phys. Rev. A* **82**, 033412 (2010).

[7] S. E. Anderson, K. C. Younge, and G. Raithel, *Phys. Rev. Lett.* **107**, 263001 (2011).

[8] M. Viteau, M. G. Bason, J. Radogostowicz, N. Malossi, D. Ciampini, O. Morsch, and E. Arimondo, *Phys. Rev. Lett.* **107**, 060402 (2011).

[9] T. Macrì and T. Pohl, *Phys. Rev. A* **89**, 011402 (2014).

[10] C. Gross and I. Bloch, *Science* **357**, 995 (2017).

[11] M. P. Fisher, P. B. Weichman, G. Grinstein, and D. S. Fisher, *Phys. Rev. B* **40**, 546 (1989).

[12] M. Greiner, O. Mandel, T. Esslinger, T. W. Hänsch, and I. Bloch, *Nature* **415**, 39 (2002).

[13] D. Jaksch and P. Zoller, *Ann. Phys. (N. Y.)* **315**, 52 (2005).

[14] M. Lewenstein, A. Sanpera, V. Ahufinger, B. Damski, A. Sen, and U. Sen, *Adv. Phys.* **56**, 243 (2007).

[15] I. Bloch, J. Dalibard, and W. Zwerger, *Rev. Mod. Phys.* **80**, 885 (2008).

[16] D. van Oosten, P. van der Straten, and H. T. C. Stoof, *Phys. Rev. A* **63**, 053601 (2001).

[17] W. Zwerger, *J. Opt. B Quantum Semiclassical Opt.* **5**, S9 (2003).

[18] M. L. Wall, A. P. Koller, S. Li, X. Zhang, N. R. Cooper, J. Ye, and A. M. Rey, *Phys. Rev. Lett.* **116**, 035301 (2016).

[19] S. Kolkowitz, S. L. Bromley, T. Bothwell, M. L. Wall, G. E. Marti, A. P. Koller, X. Zhang, A. M. Rey, and J. Ye, *Nature* **542**, 66 (2017).

[20] L. Zhang and X.-J. Liu, in *Synth. Spin-Orbit Coupling Cold Atoms* (WORLD SCIENTIFIC, 2018) pp. 1–87.

[21] P. Sengupta, L. P. Pryadko, F. Alet, M. Troyer, and G. Schmid, *Phys. Rev. Lett.* **94**, 207202 (2005).

[22] V. W. Scarola, E. Demler, and S. Das Sarma, *Phys. Rev. A* **73**, 051601 (2006).

[23] G. G. Batrouni, F. Hébert, and R. T. Scalettar, *Phys. Rev. Lett.* **97**, 087209 (2006).

[24] C. Menotti, C. Trefzger, and M. Lewenstein, *Phys. Rev. Lett.* **98**, 235301 (2007).

[25] S. Yi, T. Li, and C. P. Sun, *Phys. Rev. Lett.* **98**, 260405 (2007).

[26] M. Iskin and J. K. Freericks, *Phys. Rev. A* **79**, 053634 (2009).

[27] M. Iskin, *Phys. Rev. A* **83**, 051606 (2011).

[28] W. Li, L. Hamadeh, and I. Lesanovsky, *Phys. Rev. A* **85**, 053615 (2012).

[29] R. Landig, L. Hruba, N. Dogra, M. Landini, R. Mottl, T. Donner, and T. Esslinger, *Nature* **532**, 476 (2016).

[30] Y. Li, A. Geißler, W. Hofstetter, and W. Li, *Phys. Rev. A* **97**, 023619 (2018).

[31] V. Alba, M. Haque, and A. M. Läuchli, *Phys. Rev. Lett.* **110**, 260403 (2013).

[32] R. Islam, R. Ma, P. M. Preiss, M. Eric Tai, A. Lukin, M. Rispoli, and M. Greiner, *Nature* **528**, 77 (2015).

[33] N. Goldman, J. C. Budich, and P. Zoller, *Nat. Phys.* **12**, 639 (2016).

[34] M. Lohse, C. Schweizer, O. Zilberberg, M. Aidelsburger, and I. Bloch, *Nat. Phys.* **12**, 350 (2016).

[35] B. Wu and Q. Niu, *New J. Phys.* **5**, 104 (2003).

[36] A. Tomadin, R. Mannella, and S. Wimberger, *Phys. Rev. A* **77**, 013606 (2008).

[37] H. Deng, H. Dai, J. Huang, X. Qin, J. Xu, H. Zhong, C. He, and C. Lee, *Phys. Rev. A* **92**, 023618 (2015).

[38] W. H. Zurek, U. Dorner, and P. Zoller, *Phys. Rev. Lett.* **95**, 105701 (2005).

[39] J. Dziarmaga, M. Tylutki, and W. H. Zurek, *Phys. Rev. B* **86**, 144521 (2012).

[40] A. del Campo and W. H. Zurek, *Int. J. Mod. Phys. A* **29**, 1430018 (2014).

[41] K. Shimizu, Y. Kuno, T. Hirano, and I. Ichinose, *Phys. Rev. A* **97**, 033626 (2018).

[42] K. Shimizu, T. Hirano, J. Park, Y. Kuno, and I. Ichinose, *New J. Phys.* **20**, 083006 (2018).

[43] K. Shimizu, T. Hirano, J. Park, Y. Kuno, and I. Ichinose, *Phys. Rev. A* **98**, 063603 (2018).

[44] W. Weiss, M. Gerster, D. Jaschke, P. Silvi, and S. Montangero, *Phys. Rev. A* **98**, 063601 (2018).

[45] S. Scherg, T. Kohlert, J. Herbrych, J. Stolpp, P. Bordia, U. Schneider, F. Heidrich-Meisner, I. Bloch, and M. Aidelsburger, *Phys. Rev. Lett.* **121**, 130402 (2018).

[46] P. T. Brown, D. Mitra, E. Guardado-Sánchez, R. Nourafkan, A. Reymbaut, C.-D. Hébert, S. Bergeron, A.-M. S. Tremblay, J. Kokalj, D. A. Huse, P. Schauß, and W. S. Bakr, *Science* **363**, 379 (2019).

[47] C. J. Fujiwara, K. Singh, Z. A. Geiger, R. Senaratne, S. V. Rajagopal, M. Lipatov, and D. M. Weld, *Phys. Rev. Lett.* **122**, 010402 (2019).

[48] J. Léonard, A. Morales, P. Zupancic, T. Donner, and T. Esslinger, *Science* **358**, 1415 (2017).

[49] M. Di Liberto, A. Recati, N. Trivedi, I. Carusotto, and C. Menotti, *Phys. Rev. Lett.* **120**, 073201 (2018).

[50] A. Eckardt, C. Weiss, and M. Holthaus, *Phys. Rev. Lett.* **95**, 260404 (2005).

[51] C. Gaul, R. P. A. Lima, E. Díaz, C. A. Müller, and F. Domínguez-Adame, *Phys. Rev. Lett.* **102**, 255303 (2009).

[52] A. G. Green and S. L. Sondhi, *Phys. Rev. Lett.* **95**, 267001 (2005).

[53] A. Polkovnikov, K. Sengupta, A. Silva, and M. Vengalattore, *Rev. Mod. Phys.* **83**, 863 (2011).

[54] M. P. Kennett, *ISRN Condens. Matter Phys.* **2013**, 1 (2013).

[55] J. K. Freericks and H. Monien, *EPL* **26**, 545 (1994).

[56] V. F. Elesin, V. A. Kashurnikov, and Openov L. A., *JETP Lett.* **60**, 177 (1994).

[57] S. Fölling, F. Gerbier, A. Widera, O. Mandel, T. Gericke, and I. Bloch, *Nature* **434**, 481 (2005).

[58] T. D. Kühner, S. R. White, and H. Monien, *Phys. Rev. B* **61**, 12474 (2000).

[59] D. Rossini and R. Fazio, *New J. Phys.* **14**, 065012 (2012).

[60] K. Góral, K. Rzżewski, and T. Pfau, *Phys. Rev. A* **61**, 051601 (2000).

[61] A. Griesmaier, J. Werner, S. Hensler, J. Stuhler, and T. Pfau, *Phys. Rev. Lett.* **94**, 160401 (2005).

[62] M. Lu, N. Q. Burdick, S. H. Youn, and B. L. Lev, *Phys. Rev. Lett.* **107**, 190401 (2011).

[63] K. Aikawa, A. Frisch, M. Mark, S. Baier, A. Rietzler, R. Grimm, and F. Ferlaino, *Phys. Rev. Lett.* **108**, 210401 (2012).

[64] H. P. Büchler, A. Micheli, and P. Zoller, *Nat. Phys.* **3**, 726 (2007).

[65] A. Micheli, G. K. Brennen, and P. Zoller, *Nat. Phys.* **2**, 341 (2005).

[66] S. Kotochigova and E. Tiesinga, *Phys. Rev. A* **73**, 041405 (2006).

[67] A. V. Gorshkov, S. R. Manmana, G. Chen, J. Ye, E. Demler, M. D. Lukin, and A. M. Rey, *Phys. Rev. Lett.* **107**, 115301 (2011).

[68] S. Baier, M. J. Mark, D. Petter, K. Aikawa, L. Chomaz, Z. Cai, M. Baranov, P. Zoller, and F. Ferlaino, *Science* **352**, 201 (2016).

[69] J. Honer, H. Weimer, T. Pfau, and H. P. Büchler, *Phys. Rev. Lett.* **105**, 160404 (2010).

[70] J. B. Balewski, A. T. Krupp, A. Gaj, S. Hofferberth, R. Löw, and T. Pfau, *New J. Phys.* **16**, 063012 (2014).

[71] Y.-Y. Jau, A. M. Hankin, T. Keating, I. H. Deutsch, and

G. W. Biedermann, *Nat. Phys.* **12**, 71 (2016).

[72] J. Zeiher, R. van Bijnen, P. Schauß, S. Hild, J.-y. Choi, T. Pohl, I. Bloch, and C. Gross, *Nat. Phys.* **12**, 1095 (2016).

[73] R. Mukherjee, T. C. Killian, and K. R. A. Hazzard, *Phys. Rev. A* **94**, 053422 (2016).

[74] N. Henkel, R. Nath, and T. Pohl, *Phys. Rev. Lett.* **104**, 195302 (2010).

[75] G. Pupillo, A. Micheli, M. Boninsegni, I. Lesanovsky, and P. Zoller, *Phys. Rev. Lett.* **104**, 223002 (2010).

[76] Y. Chougale and R. Nath, *J. Phys. B* **49**, 144005 (2016).

[77] M. Greiner, O. Mandel, T. W. Hänsch, and I. Bloch, *Nature* **419**, 51 (2002).

[78] E. Altman, E. Demler, and M. D. Lukin, *Phys. Rev. A* **70**, 013603 (2004).

[79] T. Rom, T. Best, D. Van Oosten, U. Schneider, S. Fölling, B. Paredes, and I. Bloch, *Nature* **444**, 733 (2006).

[80] T. Jeltes, J. M. McNamara, W. Hogervorst, W. Vassen, V. Krachmalnicoff, M. Schellekens, A. Perrin, H. Chang, D. Boiron, A. Aspect, and C. I. Westbrook, *Nature* **445**, 402 (2007).

[81] E. Toth, A. M. Rey, and P. B. Blakie, *Phys. Rev. A* **78**, 013627 (2008).

[82] A. Hu, L. Mathey, C. J. Williams, and C. W. Clark, *Phys. Rev. A* **81**, 063602 (2010).

[83] A. M. Rey, K. Burnett, R. Roth, M. Edwards, C. J. Williams, and C. W. Clark, *J. Phys. B* **36**, 825 (2003).

[84] T. Macrì, F. Maucher, F. Cinti, and T. Pohl, *Phys. Rev. A* **87**, 061602 (2013).

[85] C.-H. Hsueh, T.-C. Lin, T.-L. Horng, and W. C. Wu, *Phys. Rev. A* **86**, 013619 (2012).

[86] S. Komineas and N. R. Cooper, *Phys. Rev. A* **75**, 023623 (2007).

[87] A. Boudjemâa and G. V. Shlyapnikov, *Phys. Rev. A* **87**, 025601 (2013).

[88] B. Capogrosso-Sansone, S. G. Söyler, N. Prokof'ev, and B. Svistunov, *Phys. Rev. A* **77**, 015602 (2008).

[89] W. Krauth, M. Caffarel, and J.-P. Bouchaud, *Phys. Rev. B* **45**, 3137 (1992).

[90] G. Seibold and J. Lorenzana, *Phys. Rev. Lett.* **86**, 2605 (2001).

[91] M. Schiró and M. Fabrizio, *Phys. Rev. Lett.* **105**, 076401 (2010).

[92] E. von Oelsen, G. Seibold, and J. Bünenmann, *New J. Phys.* **13**, 113031 (2011).

[93] R. Roth and K. Burnett, *Phys. Rev. A* **67**, 031602 (2003).

[94] B. Damski, J. Zakrzewski, L. Santos, P. Zoller, and M. Lewenstein, *Phys. Rev. Lett.* **91**, 080403 (2003).

[95] N. Elstner and H. Monien, *Phys. Rev. B* **59**, 12184 (1999).

[96] M. Hohenadler, M. Aichhorn, S. Schmidt, and L. Pollet, *Phys. Rev. A* **84**, 041608 (2011).

[97] I. Spielman, W. Phillips, and J. Porto, *Phys. Rev. Lett.* **98**, 080404 (2007).